Study of stress distribution and stress concentration factor in notched wood pieces with cohesive surfaces

Journal:	*Wood Science and Technology*
Manuscript ID:	Draft
Manuscript Type:	Original
Date Submitted by the Author:	n/a
Complete List of Authors:	AIRA, José-Ramón; Technical University of Madrid, Department of Building and Rural Roads DESCAMPS, Thierry; University of Mons, Department of Structural Mechanics and Civil Engineering NOËL, Jérôme; University of Mons, Department of Structural Mechanics and Civil Engineering
Keywords:	Cohesive Surfaces, FEM, Stress Concentration Factor, Notched Wood Pieces, ASTM D 143:94

"Study of stress distribution and stress concentration factor in notched wood pieces with cohesive surfaces"

Aira J.R.[1], Descamps T.[2], Noël J.[3]

[1] Researcher. Department of Building and Rural Roads. Technical University of Madrid.
email: joseramonaira@gmail.com
[2] Professor. URBAINE, Dept. Structural Mech. and Civil Eng., University of Mons, Mons, Belgium.
email: Thierry.DESCAMPS@umons.ac.be
[3] Assistant Professor. URBAINE, Dept. Structural Mech. and Civil Eng., University of Mons, Mons, Belgium.
email: Jerome.NOEL@umons.ac.be

Abstract

In this study the stress distribution and stress concentration factor (SCF) of a generic notched wood piece and ASTM D 143:94 notched shear block specimen are analyzed. A 2D plane stress finite element model with linear elastic behaviour was assumed for the bulk material and it was considered a predefined potential crack path and cohesive behaviour of the crack surfaces. Wood was considered as an orthotropic material with transversal isotropy. In the notched wood pieces, the shear stress distribution along the shear plane and the SCF when varying the ratio *l/t* (length of the heel/depth of the notch) was obtained. The shear stress distribution is not uniform in any situation getting closer to a slightly triangular shape. The shear stress concentration increases when *l/t* is greater and for $l/t > 8$ the failure occurs due to crack progressing. The SCF can be approximated fairly well to the natural logarithm of *l/t*. In the ASTM D 143:94 notched shear block specimen, the shear stress distribution remains a constant value only in the central part of the shear plane and the SCF is 2,41.

Keywords

Cohesive Surfaces, FEM, Stress Concentration Factor, Notched Wood Pieces, ASTM D 143:94.

1. Introduction

Timber frameworks are one of the most important and widespread typology of timber structures. Their configurations and joints are most of the time complex and testify to a high technical nature and an excellent understanding of the structural behaviour. Today, thanks to the advent of CNC wood-processing machinery, this kind of joints knows a renewed interest. Traditional carpentry joints connect timber elements, usually subjected to compressive axial loads, often without any other devices. Because of their complex shapes with notches directly cut in wood, traditional joints may exhibit a bending stiffness and are able to transfer a bending moment. In such connections, the transfer of loads is possible through direct contact and friction that induce a complex stress state in wood (axial and shear stresses). Hence, the ultimate design is often limited to the check the weakest point, e.g. the shear strength of some planes in the joint (figure 1).

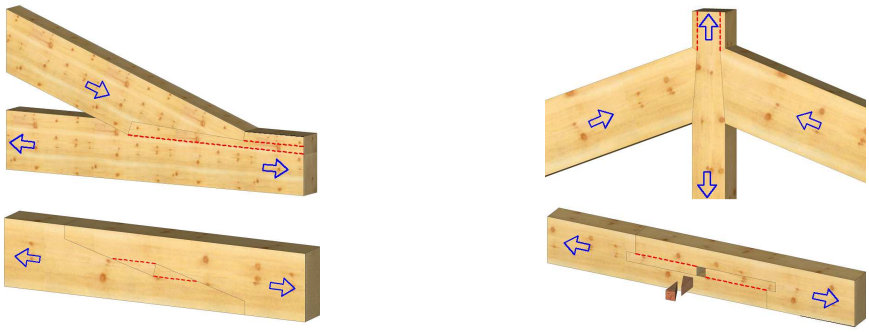

Figure 1. Examples of traditional joints where it is necessary to verify the shear strength (shear plane in red)

German norm DIN 1052:2008 [1] allows considering a uniform distribution of shear stress in the heel of the joint. This assumption is possible when the length of the heel is shorter than 8 times the depth of the notch. Considering higher values of the length does not increase the shear strength of the section. Actually, shear stress distribution is of course not uniform in any situation because of a stress concentration occurs at the beginning of the heel.

On the other hand, the American Society of Testing and Materials proposed since many decades to use notched shear block specimen (ASTM D 143:94) [2] to characterize the parallel to grain shear strength of solid wood, figure 2.

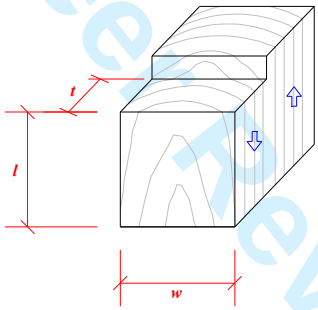

Figure 2. ASTM D 143:94 notched shear block specimen

The failure load, P_{max}, is used as an estimate of ultimate shear strength, $\tau_{nominal}$, along the shear plane. Thereby, shear strength is obtained considering uniform stress distribution by dividing the load of failure by the area of the shear plane.

$$\tau_{nominal} = \frac{P_{max}}{w \cdot l}$$

where,

$\tau_{nominal}$	shear strength (N/mm^2);
P_{max}	maximum applied load (N);
w	width of the shear plane (mm);
l	length of the shear plane (mm).

According to many researchers, the shear strength determined from this test have been shown to be lower than the actual shear strength of wood what is mainly due to the real non-uniform

Editorial Office, TU München, Holzforschung München, Winzererstr. 45, 80797 München, Germany

stress distribution over the failure plane and stress concentrations at the re-entrant corner of the notch. Coker and Coleman [3] determined that the stress concentration factor (SCF) was at least 2 by performing photo-elastic experiments with xylonite (considered here as an isotropic material). Raddcliffe and Suddarth [4] showed experimentally an unsymmetrical stress distribution with SCF to be approximately 2 by using strain gages. Cramer et al. [5] used a two-dimensional orthotropic finite element analysis and determined a SCF of 2,36; numerical results was higher than experimental ones due to crushing and splitting occurs near the notch. Moses and Prion [6] used a three-dimensional finite element analysis taking into account anisotropic and bilinear material (in compression), brittle failure was predicted using the Weibull weakest link theory. Their model strength predictions were found to be approximately 1,7 times greater than nominal shear strength and SCF to be at least 2. Dahl and Malo [7] indicated that during the test, a state of pure shear does not occur since the eccentricity of loading causes a bending moment appearing normal stresses perpendicular to the shear plane, therefore they considered the Arcan test most appropriate for a general study of the shear properties of wood.

Within the context of linear elasticity theory, an abrupt change of material section caused by a sharp notch produces a stress singularity at the re-entrant corner of the notch. In this singular point, the stress distribution is asymptotic to infinity when refining the finite element mesh, consequently SCF (defined by peak stress divided by nominal stress) is highly dependent on the mesh size [8]. In this regard, Gustafsson and Enquist [9] indicated that Weibull theory and conventional stress analysis cannot be applied to strength analysis of structural elements with a stress singularity caused by a crack or a sharp notch.

The theory of linear elastic fracture mechanics (LEFM) has been largely used in timber design problems to analyze cracking and crack propagation. However, as it based on the assumption of an ideal linear elastic material and the pre-existence of a crack, it gives accurate results only for the structural elements where the fracture process zone (FPZ) is small compared with the length of the crack. Cohesive zone model (CZM), developed by [10, 11, 12] but quiet new in timber engineering, seems more appropriate as a theoretical basis for strength and fracture analysis of wood structural elements [13].

2. Material and Methods

The object of this paper is to analyze the stress distribution and to determine the SCF in notched wood pieces subjected to axial loads. The study extends to analysis of ASTM D 143:94 notched shear block specimen.

In recent years, the CZM has been applied to study of wood elements finding satisfactory results [14, 15, 16]. CZM approach to simulate crack initiation and propagation can be implemented in the finite element method (MEF) using the FE software ABAQUS.

In this study, we used a 2D plane stress model. Wood was considered as an orthotropic material with transversal isotropy and the values of the elastic properties perpendicular to the grain were achieved by the arithmetic average in the radial (R) and tangential (T) directions.

The parameters of the material properties are indicated in table 1. Due to the lack of complete information for the same species and origin, especially the fracture energy values for modes II and III, the parameters considered by Danielsson and Gustafsson [13] were taken into account as a reference to this work. These values are closed to the main values found in literature for Norway spruce (*Picea abies* (L.) Karst) and Scots pine (*Pinus sylvestris* L.) grown in Scandinavia.

Stiffness parameters (MPa) and Poisson´s ratios								
E_L	E_T	E_R	ν_{LT}	ν_{LR}	ν_{TR}	G_{LT}	G_{LR}	G_{TR}
12.000	650	650	0,39	0,39	0,39	700	700	50
Strength parameters (MPa)								
$f_{t,90,T}$	$f_{t,90,R}$	$f_{v,LT}$	$f_{v,LR}$	$f_{v,TR}$				
3,0	3,0	6,0	6,0	3,0				
Fracture energy (N/mm)								
G_I^C	G_{II}^C	G_{III}^C						
0,300	0,900	0,900						

Table 1. Material properties (orthotropic with transversal isotropy)

A linear elastic behaviour was assumed for the bulk material and it was considered a predefined potential crack path along the shear plane. The crack plane was modelled by 2 surfaces facing each other with cohesive behaviour. Cohesive surfaces are primarily intended for situations in which the interface thickness is negligibly small since interface thickness are not considered [17].

A progressive mesh was used and the mesh size was refined in the direction of the crack plane. Each element was modelled in ABAQUS considering the element of its internal library called CPS4R which is a 4-node plane stress quadrilateral with reduced integration. Cohesive surfaces were divided into 400 elements with homogeneous size because the accuracy depends heavily on the number of divisions (it is common to use a high number of elements) [17].

In order to obtain the SCF it is necessary to compare the maximum shear stress (τ_{max}) with nominal shear stress ($\tau_{nominal}$). Therefore, the applied load P_{max}, corresponds to the load that produce a shear stress failure along the shear plane by assuming an uniform shear stress distribution.

The first study was a notched piece subjected to uniformly distributed load P_{max} in axial direction (L). Vertical displacement at the bottom face and horizontal displacement on the left face were restricted, figure 3. This study examined a generic geometry with a notch angle of 90 degrees, since in traditional timber joints can be found notches forming different angles.

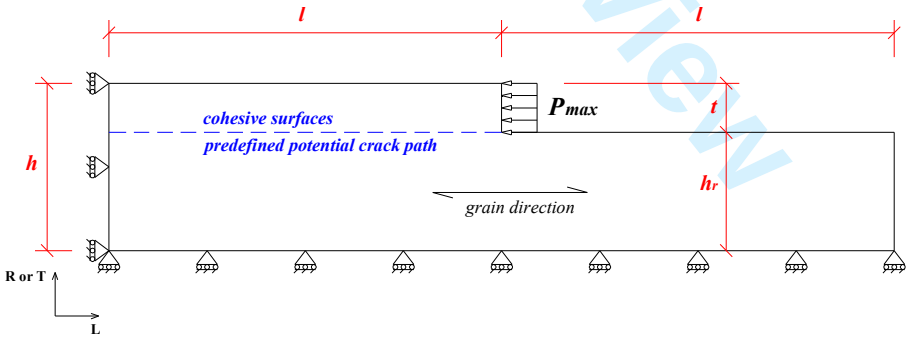

Figure 3. Notched piece subjected to axial load

The notched piece was analyzed considering 3 different lengths of the shear plane: l = 120 mm, l = 160 mm and l = 200 mm. For each value of l, the notch depth, t, was modified according to the ratios l/t = 2, l/t = 4, l/t = 6, l/t = 8, l/t = 10 and l/t = 12, table 2.

l (mm)	h_r (mm)	min mesh size (mm)	P_{max} (N)	l/t (nº elements)					
120	36	0,3	720	2 (40.480)	4 (36.080)	6 (33.680)	8 (30.480)	10 (28.480)	12 (30.448)
160	48	0,4	960	2 (45.552)	4 (41.152)	6 (37.952)	8 (37.152)	10 (34.752)	12 (37.952)
200	60	0,5	1200	2 (58.265)	4 (40.265)	6 (44.265)	8 (43.865)	10 (41.065)	12 (39.465)

Table 2. Parameters of notched piece study

After the notched piece study, the ASTM D 143:94 notched shear block specimen was analyzed by using finite element simulation of the test described by the standard. The steel test frame (base plate and loading plate) was modelled with usual steel properties (E = 210.000 MPa, G = 81.000, v = 0,3). The base plate was restricted from displacement in all directions, whereas the loading plate was only allowed to move in the direction of the applied load. Contact elements type surface-to-surface were used to introduce the effect of friction between steel and wood with a static friction coefficient of 0,7 [18]. The horizontal contact between the loading plate and wood was considered without friction because there is no external element applying pressure and contact surfaces could be out of contacting during the test, figure 4. The meshing of this study was of 87.720 elements with a smaller mesh size of 0,1 mm in the cohesive surfaces.

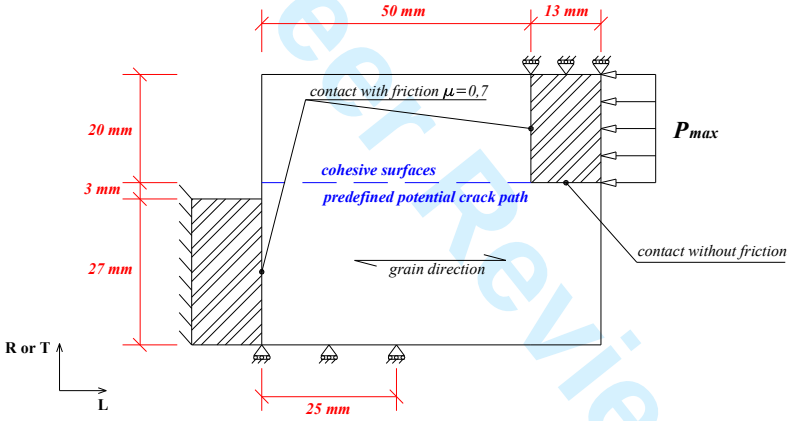

Figure 4. ASTM D 143:94 notched shear block specimen

The traction-separation model in ABAQUS assumes initially linear elastic behaviour followed by the initiation and evolution of damage. Damage initiation defines the point of initiation of stiffness degradation and begins when the contact stresses satisfy certain damage initiation criteria. In the present work, damage was assumed to initiate when the maximum nominal stress ratio reaches a value of 1. This non interactive criterion can be represented as [17],

$$\max\left\{\frac{\langle t_n \rangle}{t_n^0}, \frac{t_s}{t_s^0}, \frac{t_t}{t_t^0}\right\} = 1$$

where,

t_n component normal to the crack surface (N/mm^2);
t_s first shear direction on the crack surface (N/mm^2);

t_t	second shear direction on the crack surface (N/mm^2);
t_n^0, t_s^0, t_t^0	peak value of the nominal stress (t_n^0 = 3 N/mm^2, t_s^0 = 6 N/mm^2 and t_t^0 = 3 N/mm^2, see table 1).
< >	Macaulay bracket to avoid damage initiation by purely compressive state. Its value is 0 when $t_n < 0$ (compression), and t_n when $t_n \geq 0$.

After damage initiation, damage evolution describes the rate at which the cohesive stiffness is degraded once the corresponding criterion is reached. A scalar damage variable, D, represents the overall damage at the contact point. D initially has a value of 0 and evolves from 0 to 1 with additional loading. The contact stress components are affected by the damage according to equation $t_i = (1\text{-}D)\,t_i^e$ $(i = n,s,t)$, where t_i^e is the contact stress component predicted by the elastic traction-separation behaviour for the current separations without damage [17].

In the present work, damage evolution was defined based on the energy that is dissipated as a result of the damage process (fracture energy). A power law defines the dependence of the fracture energy of the mixed-mode fracture, and softening behaviour defines the relation between stress and fracture energy in the FPZ. The fracture energy is equal to the area under the traction-separation curve so the software ensures that this area is equal to the fracture energy for the softening function used.

At the re-entrant corner of the notch, both parallel to grain shear stress and perpendicular to grain tensile stress occurs so the piece is subjected to a mixed-mode fracture (I+II). De Moura et al. [19] determined that relation between fracture energy (I+II) are in agreement with the linear energetic criterion. Therefore a linear power law based on energy was considered in this work,

$$\left\{\frac{G_I}{G_I^C}\right\}+\left\{\frac{G_{II}}{G_{II}^C}\right\}+\left\{\frac{G_{III}}{G_{III}^C}\right\}=1$$

where,

$G_I\, G_{II}\, G_{III}$	energy release rate of the fracture modes I, II and III respectively;
G_I^C	critical fracture energy required to cause failure in the normal direction (G_I^C = 0,300 N/m, see table 1);
G_{II}^C	critical fracture energy required to cause failure in the first shear direction (G_{II}^C = 0,900 N/m);
G_{III}^C	critical fracture energy required to cause failure in the second shear direction (G_{III}^C = 0,900 N/m);

For quasi-brittle materials as wood the most used damage laws are linear, bilinear, trilinear or exponential [20]. In order to obtain the SCF, the traction might not drop immediately after damage initiation, so an exponential damage evolution with evolution based on energy (exponential softening) was used in the present work. According with this criterion, the parameter D is obtained as [17],

$$D=\int_{\delta_0}^{\delta_f}\frac{T_{eff}\cdot d\delta}{G^C-G_0}$$

where,

T_{eff}	effective traction;
δ	effective separation;

G^C critical fracture energy required to cause failure;
G_0 elastic energy at damage initiation.

In this way, after the damage initiation occurs, it is possible to obtain higher stresses than nominal stresses (t_n^0, t_s^0, t_t^0) due to the FPZ is only governed by the energy criteria (power law and softening function). The SCF is obtained just by dividing the maximum shear stress by nominal shear stress.

Finally, some difficulties of convergence were found in the notched piece study, so to overcome these difficulties it was necessary to introduce a viscous regularization of the constitutive equations defining cohesive behaviour implemented in ABAQUS (stabilization). The viscosity coefficient value was 0,001 to all of the situations except to l/t = 12 (l = 200 and l = 160) where a value of 0,005 was considered.

3. Results and Discussions

Below are shown the results of the notched piece study considering the 3 different lengths of the shear plane and the ASTM D143:94 notched shear block specimen study.

3.1. Notched piece

The stress map of the notched piece, with parallel to grain shear stress and perpendicular to grain tensile stress, is shown in figure 5.

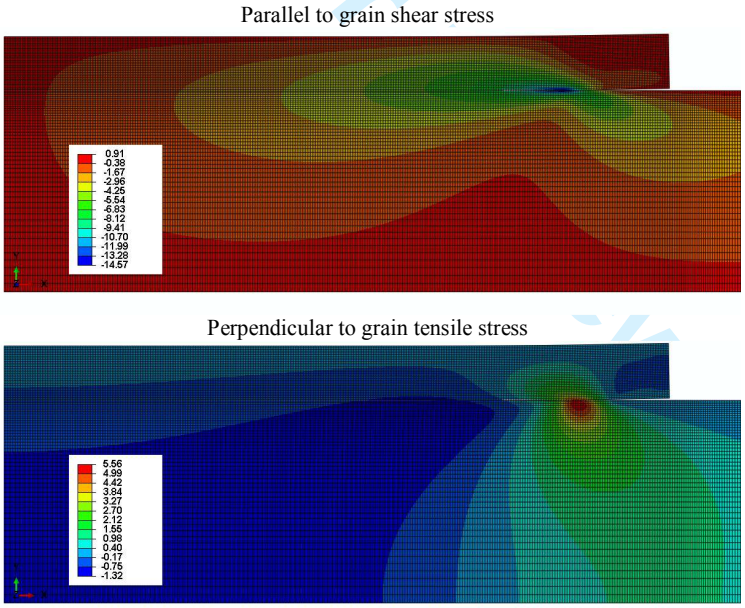

Figure 5. Stress map of notched piece (l=160 mm, l/t=12). Deformation x2

It is observed that a stress concentration occurs into the FPZ over the potential crack path. The vertical displacement of loaded surface is not restricted so, in the particular situation shown, the crack has propagated due to mixed-mode fracture process when damage evolution is finished.

Editorial Office, TU München, Holzforschung München, Winzererstr. 45, 80797 München, Germany

To compare the stress distribution in the shear plane (potential crack path), a graph with Cartesian axes was made, figure 6. The graph shows the stress distribution obtained by finite elements analysis along the potential crack path. The horizontal axis represents the length of potential crack path in mm, and the vertical axis represents the parallel to grain shear stress and perpendicular to grain tensile stress in N/mm^2.

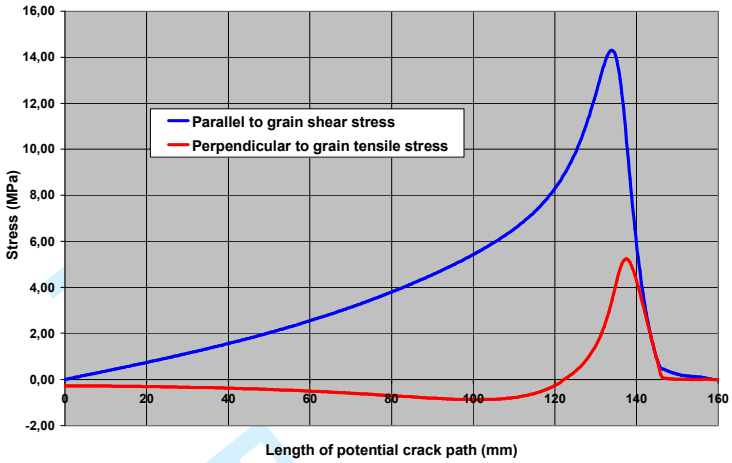

Figure 6. Stress distribution of notched piece (l=160 mm, l/t=12)

In all the studied situations, damage initiation begins due to the perpendicular tensile stress reaches the peak value of the nominal stress (t_n^0 = 3 N/mm^2) before shear stress does (t_s^0 = 6 N/mm^2). Furthermore, the peak shear stress is always higher than peak tensile stress. In the particular situation of the graph (*l = 160 mm, l/t = 12*), the stress drops to zero resulting in the propagation of the crack.

In order to study the shear stress distribution in relation to the ratio *l/t*, 3 graphs were made considering the 3 different lengths of the shear plane, figure 7. The graphs show the shear stress distribution along the potential crack path for different values of *l/t*. The horizontal axis represents the length of potential crack path in mm, and the vertical axis represents the parallel to grain shear stress in N/mm^2.

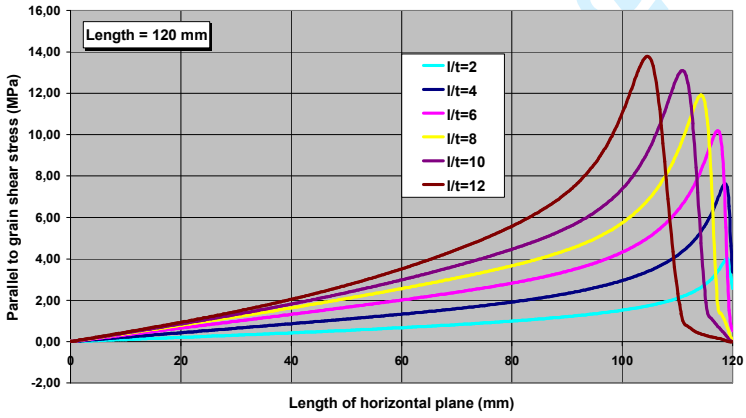

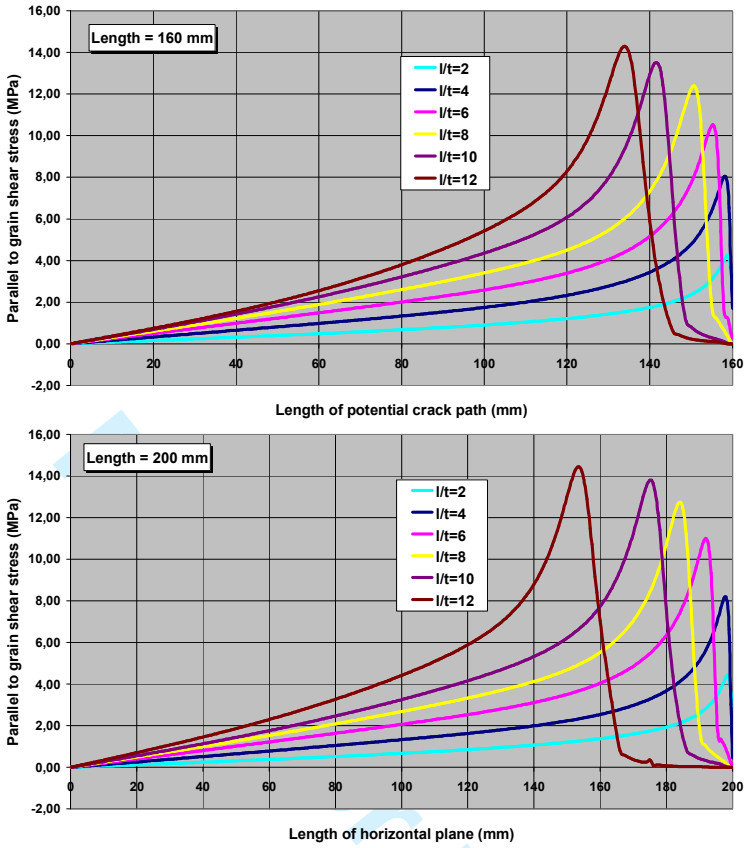

Figure 7. Shear stress distribution of notched piece

For values of the ratio l/t = 10 and l/t = 12, the shear stress reaches zero before the final part of the shear plane (beginning of the heel). For these values, damage evolution process is completed and the crack has progressed. For the value of $l/t = 8$, the shear stress drops to zero just at the final part of the shear plane, and for lower values of l/t, shear stress is still higher than zero.

On the other hand, the fracture progress in RL (crack plane is perpendicular to R direction and the crack propagates in L direction) or TL (crack plane is perpendicular to T direction and the crack propagates in L direction) directions, responds to a semi-brittle behaviour [14]. Accordingly, the crack propagation after damage evolution (in RL or RT directions) due to parallel to grain shear stress does not occur, so it is considered that the failure of the shear plane occurs when the crack begins to progress, i.e. for values of $l/t > 8$. Aira [21] obtained by means of experimental testing of halved and tabled timber scarf joint that shear strength does not increase when $l/t > 8$. This result is consistent with the guidelines of the German standard DIN 1052:2008 [1], which indicates that for values of $l > 8 \cdot t$ an increase of the length of shear plane does not correspond to an increase in shear strength (so if you need a higher capacity, you should only increase the width of the shear plane).

Moreover, when decreasing the ratio l/t, the peak shear stress decreases too because for higher value of the notch depth, t, the applied load P_{max} is distributed on a major cross-section and so the shear stress concentration at the notch becomes smaller.

To obtain the SCF to different values of l/t, a new graph was made, figure 8. The horizontal axis represents the values of l/t, and the vertical axis represents the values of the SCF.

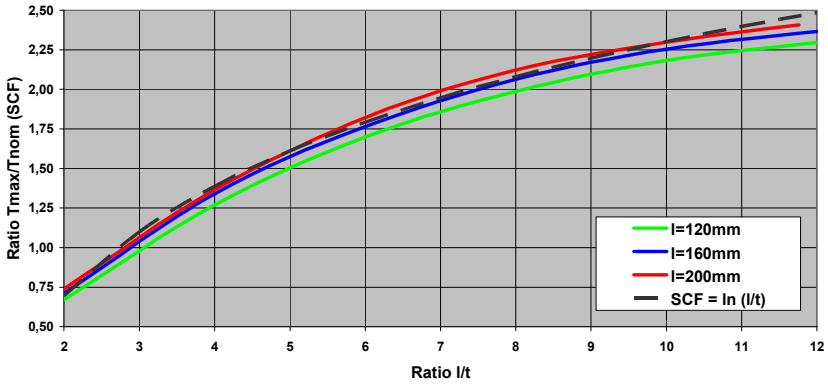

Figure 8. SCF to different values of the ratio l/t

The SCF distribution is very similar for the 3 situations studied. SCF value increases with the value of *l/t* however the increase is not linear. When *l/t* = 3, the SCF is closed to 1, and the same way, when *l/t* = 8 the SCF is closed to 2. Furthermore, the SCF evolution versus *l/t* can be approximated fairly well by a simple logarithmic function:

$$SCF = \ln\left(l/t\right)$$

This equation is very interesting as it can be easily used for the design of notched pieces similar to those analyzed. This approach, closer to the real behaviour of the specimen, provides a better understanding of shear failure and could be favourably used for the design.

3.2. ASTM D 143:94 notched shear block specimen

The same numerical procedure was used to analyze the shear stress distribution of the ASTM D 143:94 notched shear block specimen. The shear stress map is shown in figure 9.

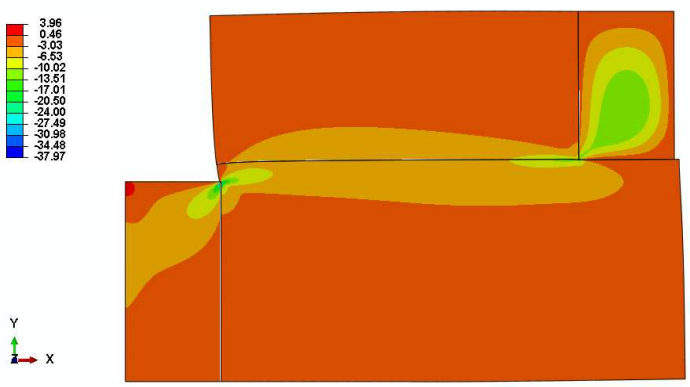

Figure 9. Shear stress map of the ASTM D 143:94 notched shear block specimen. Deformation x10

A shear stress concentration occurs in the upper area of contact between the recessed steel plate and the wooden specimen. Stress concentration occurs outside the considered shear plane because the steel plate is positioned 3 mm below. Another shear stress concentration occurs at

the bottom of the contact area between wood and the movable steel plate. This stress concentration cannot be avoided because the steel plate directly affects the shear plane.

On the figure 10, the shear stress distribution along the shear plane is shown. The graph indicates the numerical shear stress distribution obtained by FEM and the nominal shear stress distribution considered by standard ASTM D 143:94. The horizontal axis represents the length of potential crack path in mm, and the vertical axis represents the parallel to grain shear stress in N/mm^2.

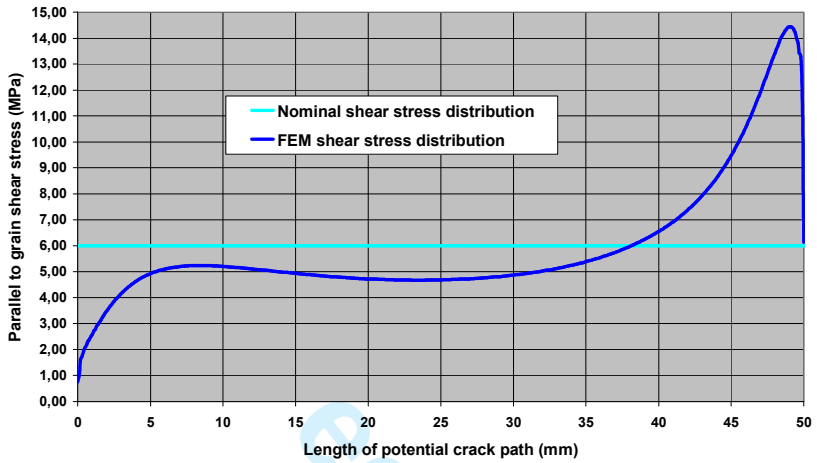

Figure 10. Shear stress distribution of the ASTM D 143:94 notched shear block specimen

In the initial part of the shear plane, the FEM shear stress increases quickly from zero until the value of 5 N/mm^2 which remains slightly constant in the central part. Nevertheless, in this part the FEM shear stress is lower than nominal shear stress ($\tau_{nominal}$ = 6 N/mm^2). In the final part, the shear stress increases quickly until reaching its maximum value (τ_{max} = 14,44 N/mm^2). Then, the shear stress reduces again during the softening process of damage evolution.

Finally, the SCF in the ASTM D 143:94 notched shear block specimen was obtained applying the relation,

$$SCF_{ASTM} = \frac{\tau_{max}}{\tau_{nom}} = \frac{14{,}44}{6} = 2{,}41$$

As noted in the introduction section, many researchers determined that the SCF was at least 2. Taking into account cohesive surfaces behaviour the exact value of 2,41 was obtained. However, this value may overestimate the real one as the numerical model do not consider any plastic behaviour (e.g. for compression and shear) [22, 23].

4. Conclusions

Finite element models of a generic notched wood piece and of the shear specimen defined by ASTM D 143:94 have been made. Considering a predefined potential crack path and a cohesive behaviour of the crack surfaces, the stress distribution and the SCF have been analysed and defined.

When notched piece was subjected to the nominal load, P_{max}, for values of $l/t > 8$, the failure occurred due to the progress of the crack. This result complies well with the guidelines of the German standard DIN 1052:2008. The same standard also allows considering a uniform shear stress distribution for values of $l/t \leq 8$, nevertheless, the distribution is not uniform getting closer to a slightly triangular shape where the maximum value is determined by the SCF. Finally, the SCF was obtained as a function of l/t, so, for the studied geometries, the SCF can be approximated fairly well with the natural logarithm of l/t.

Shear stress distribution along the shear plane of ASTM D 143:94 notched shear block specimen is not uniform, keeping a constant value only in the central part of the section. In addition, the SCF that occurs in the test was calculated resulting a value of 2,41.

Acknowledgements

This research has been finalized during a Short Term Scientific Mission performed by Mr. José-Ramon Aira at the University of Mons. All the authors would like to thanks the European Cooperation in Science and Technology and in particular the Action COST FP1101 "Assessment, Reinforcement and Monitoring of Timber Structure" for their financial support.

References

[1] DIN 1052:2008. "Design of timber structures. General rules and rules for buildings".
[2] ASTM D143:94. "Standard methods of testing. Small clear specimens of timber".
[3] Coker E.G. and Coleman G.P (1935). "Photo-elastic investigation of shear tests of timber". Selected Engineering Pap. No. 174. The Institution of Civil Engineers. London, England.
[4] Radcliffe B.M. and Suddarth S.K. (1955). "The notched beam shear test for wood". Forest Prod. J. 5(2):131-135.
[5] Cramer S.M., Goodman J.R., Bodig J. and Smith F.W. (1984). "Failure modeling of wood structural members". Structural Res. No. 51, Civil Engineering Dept., Colorado State Univ., Fort Collins, CO.
[6] Moses D.M. and Prion H.G.L. (2002). "Anisotropic plasticity and the notched wood shear block". Forest Products Journal, 52, 6. Pg. 43.
[7] Dahl K.B. and Malo K.A. (2009). "Linear elastic properties of spruce softwood". Wood Sci Technol, 43:499-525.
[8] Aira J.R., Arriaga F., Íñiguez-González G., Guaita M. and Esteban M. (2012). "Analysis of the stress state of a halved and tabled traditional timber scarf joint with the finite element method". WCTE 2012, World Conference on Timber Engineering. Auckland, New Zealand.
[9] Gustafsson P.J. and Enquist B. (1988). "Träbalks Hållfasthet vid rätvinklig urtagning". Report TVSM-7042. Division of Structural Mechanics. Lund University.
[10] Barenblatt G.I. (1962). "The mathematical theory of equilibrium cracks in brittle fracture". Adv Appl Mech, 7:55-129.
[11] Dugdale D.S. (1960). "Yielding of steel sheets containing slits". J. Mech Phys Solids, 8:100-4.
[12] Hillerborg A., Modée M. and Peterson P.E. (1976). "Analysis of crack formation and crack growth in concrete by means of fracture mechanics and finite elements". Cement and Concrete Research, Vol. 6, pp. 773-782.

[13] Danielsson H. and Gustafsson P.J. (2013). "A three dimensional plasticity model for perpendicular to grain cohesive fracture in wood". Engineering Fracture Mechanics, 98:137-152.
[14] Smith I., Landis E. and Gong M. (2003). "Fracture and Fatigue in Wood". Wiley Editorial. England. 234p.
[15] Stefansson F. (2001). "Fracture Analysis of Orthotropic Beams". Lund University. Licenciate Dissertation.
[16] Boström L. (1992). "Method for determination of the softening behaviour of wood and the applicability of a nonlinear fracture mechanics model". Doctoral Thesis. Report TVBM-1012, Lund, Sweden.
[17] ABAQUS/CEA Version 6.11 Standard Manual (2011). Dassault Systèmes Simulia Corp.Providence, Rhode Island, U.S.A.
[18] Smith I. (1983). "Coefficient of friction values applicable to contact surfaces between mild steel connectors such us bolts and dry European white wood". Journal of the Institute of Wood Science. 229-234.
[19] De Moura M.F.S.F., Oliveira J.M.Q., Morais J.J.L. and Dourado, N. (2011). "Mixed mode (I+II) fracture characterization of wood bonded joints". Constructions and Building Materials. 1956-1962.
[20] Fortino, S., Zagari G., Mendicino A.L. and Dill-Langer G. (2012). "A simple approach for FEM simulation of Mode I cohesive crack growth in glued laminated timber under short-term loading". Rakenteiden Mekaniikka (Journal of Structural Mechanics). Vol. 45, No 1, pp. 1-20.
[21] Aira J.R. (2013). "Experimental and FEM analysis of the stress state of halved and tabled traditional timber scarf joint". Doctoral Thesis. Department of Building and Rural Roads. Technical University of Madrid. Spain.
[22] Dahl K.B. and Malo K.A. (2009). "Nonlinear shear properties of spruce softwood: experimental results". Wood Sci Technol, 43:539-558.
[23] Dahl K.B. and Malo K.A. (2009). "Nonlinear shear properties of spruce softwood: Numerical analyses of experimental results". Composites Science and Technology, 69:2144-2151.